Regimes of Thermocline Scaling: The Interaction of Wind Stress and Surface Buoyancy

PAOLA CESSI

Scripps Institution of Oceanography, University of California, San Diego, La Jolla, California

(Manuscript received 24 June 2006, in final form 9 November 2006)

ABSTRACT

The role of the relative geometry of mechanical forcing (wind stress) and buoyancy forcing (prescribed surface temperature) in the maintenance of the main thermocline is explored. In particular, the role of the wind stress curl in enhancing or suppressing the generation of baroclinic eddies is studied in simplified domains. The dependence of key quantities, such as the depth of the thermocline and the maximum heat transport, on the external parameters such as diapycnal mixing and dissipation rate is examined. Qualitatively different regimes are found depending on the relative phase of the wind stress and surface buoyancy distribution. The most efficient arrangement for eddy generation has Ekman pumping (suction) in conjunction with high (low) surface buoyancy. This corresponds to the situation found in the midlatitudes, where the surface Ekman flow carries heat toward the warmer region (i.e., upgradient of the surface temperature). In this case, strong eddy fluxes are generated in order to counteract the upgradient heat transport by the Ekman cell. The result is a thermocline whose depth is independent of the diapycnal diffusivity. However, the competition between these opposing heat fluxes leads to a weak net heat transport, proportional to the diffusivity responsible for the diabatic forcing. This arrangement of wind stress provides a large source of available potential energy on which eddies can grow, so the mechanical energy balance for the eddies is consistent with a substantial eddy heat flux. When the same surface temperature distribution is paired with the opposite wind stress curl, the mean flow produces a sink, rather than a source, of available potential energy and eddies are suppressed. With this arrangement, typical of low latitudes and the subpolar regions, the Ekman overturning cell carries heat downgradient of the surface temperature. Thus, the net heat transport is almost entirely due to the Ekman flow and is independent of the diapycnal diffusivity. At the same time the thermocline is a thin, diffusive boundary layer. Quantitative scalings for the thermocline depth and the poleward heat transport in these two limiting cases are contrasted and successfully compared with eddy-resolving computations.

1. Introduction

Recent global observations using satellite altimetry (Maximenko et al. 2005; Stammer et al. 2006) reveal eddies with scales on the order of (but larger than) the first baroclinic deformation radius throughout the ocean, with energy maxima in the subtropics, the equatorward side of the Antarctic Circumpolar Current (ACC) region and the equator. Corresponding minima are found in the subpolar region and in the Tropics. While the near-equator mesoscale activity could be due to barotropic instability of the equatorial current system, elsewhere the observed anomalies in sea surface height are most likely due to finite-amplitude equilibration of eddies resulting from baroclinic instability of the large-scale currents (Richards et al. 2006).

At the moment, models used to make climate predictions cannot adequately resolve the first baroclinic deformation radius, especially in high latitudes, despite the observational evidence that eddies are ubiquitous in the ocean. A partial remedy is to parameterize the eddy fluxes of heat and momentum. To test their accuracy, parameterizations must be evaluated quantitatively against direct simulations or observations, and both of these evaluations are only possible on regional scales. An implicit assumption is that the same parameterizations will be accurate in different regions and under different climatic conditions.

With these premises it is natural to ask the following questions: What are the conditions that favor or even necessitate eddies in the ocean? In particular, what

Corresponding author address: Paola Cessi, Scripps Institution of Oceanography, University of California, San Diego, 9500 Gilman Dr., UCSD-0213, La Jolla, CA 92093-0213.
E-mail: pcessi@ucsd.edu

DOI: 10.1175/JPO3103.1

kind of external forcing leads to vigorous eddy activity? Is there a *local* connection between surface forcing (wind stress curl and buoyancy fluxes) and the strength of mesoscale eddies? Given that baroclinic eddies are in certain cases essential for the maintenance of the mean flow, it is desirable to know in advance in what regions of the World Ocean conditions favorable to eddy activities are expected.

The ACC is an example of a region where the mean stratification and the mean zonal currents are maintained by eddy fluxes of buoyancy. Thus, modern studies of baroclinic eddies in this region focus on examining the statistics of the eddies as the forcing and dissipation are varied, rather than as a function of a specified mean state (Karsten et al. 2002; Cenedese et al. 2004; Gallego et al. 2004; Henning and Vallis 2005; Cessi et al. 2006). This is a complementary approach to examining the eddies arising from the instability of a prescribed basic flow.

Our approach is to systematically explore the configurations of the external forcing (i.e., the wind stress and the surface buoyancy distribution) that leads to a distinction between eddy-rich and eddy-poor regions. Such a qualitative difference is especially important when eddies cannot be resolved globally, or when they have to be parameterized. Most parameterizations of eddy buoyancy fluxes (Gent et al. 1995; Treguier et al. 1997) assume that eddy heat fluxes have a local dependence on the buoyancy field gradient, without any reference to whether the mechanical forcing is compatible with the production of eddies. However, the mechanical energy balance for the eddies shows that the convergence of available potential energy into eddy kinetic energy depends on the Ekman pumping (Gill et al. 1974; Cessi et al. 2006). Thus, any local eddy parameterization should be consistent with the eddy–energy balance, which we show to depend crucially on the relative phase of the Ekman pumping (or suction) and the surface buoyancy.

The problem thus posed is very complex. Our approach is to study this issue in a hierarchy of geometries of increasing complexity, beginning with simplified domains and forcing shapes, and progressing toward more realistic ones. In this study, we focus on the relative phase of the latitudinal distribution of wind stress and surface buoyancy, since these are the main forcings of oceanographic interest. We assume that wind and buoyancy forcing depend on latitude only, and have simple, large-scale sinusoidal shapes. As an initial step, we consider domains that are doubly periodic, which enables us to change the phase between the wind stress and the surface buoyancy, unencumbered by solid boundary effects. In this geometry, there is no ambiguity on how to partition the flow into eddy and mean components, since the latter is naturally defined as a zonal and time average.

The simplicity of the configuration allows us to make substantial progress and we obtain scaling laws in terms of the external parameters for two important quantities: the depth of the thermocline h and the poleward buoyancy transport $\overline{vb}$. These theoretical predictions compare well to direct numerical simulations.

2. The model

The model is

$$\frac{Du}{Dt} - fv + p_x = \boldsymbol{\nabla}\cdot\nu\boldsymbol{\nabla}u + \delta_s^{-1}\gamma_s\tau_s - r\gamma_b u,$$

$$\frac{Dv}{Dt} + fu + p_y = \boldsymbol{\nabla}\cdot\nu\boldsymbol{\nabla}v - r\gamma_b v,$$

$$p_z = b,$$

$$\frac{Db}{Dt} = \boldsymbol{\nabla}\cdot\kappa\boldsymbol{\nabla}b, \quad \text{and}$$

$$\boldsymbol{\nabla}\cdot\mathbf{u} = 0. \tag{1}$$

The velocity is $\mathbf{u} = (u, v, w)$, and the vertical coordinate is $-H < z < 0$, where H is the constant depth. The horizontal coordinates are $0 < x < L_x$ and $0 < y < L_y$. The relation between buoyancy and temperature is $b = g\alpha(T - T_o)$.

We examine a doubly periodic geometry, where periodicity is imposed in both the latitudinal as well as the longitudinal directions. This is the ideal configuration for studying the effect of a phase relation between the wind forcing $\tau_s(y)$ and the buoyancy forcing $b_s(y)$, defined later in (6). However, with a domain periodic in the meridional direction it is not possible to have a variable Coriolis parameter; thus all the calculations presented here are on the f plane.

a. Forcing and dissipation

The momentum equation is forced by a zonal stress concentrated near the surface $z = 0$. This wind stress is modeled with the body force in (1): $\delta_s^{-1}\gamma_s(z)\tau_s(y)\hat{\mathbf{x}}$. Here, $\tau_s(y)$ is a specified pattern of wind stress, and the constant $\delta_s \ll H$ is the depth of the surface layer. We use a sinusoidal wind profile:

$$\tau_s(y) = -\tau\sin(2\pi y/L_y + \phi), \tag{2}$$

where ϕ is the phase of the wind relative to the origin of the domain and $\tau > 0$ is the strength of the wind stress. The nondimensional "surface function,"

$$\gamma_s(z) \equiv \sqrt{\frac{2}{\pi}} e^{-z^2/2\delta_s^2}, \tag{3}$$

tapers the body force $\tau_s(y)$ smoothly to zero in the ocean interior. We use $\delta_s = 40$ m. The surface function γ_s is normalized so that

$$\int_{-H}^{0} \gamma_s(z)\, dz = \delta_s. \tag{4}$$

This normalization ensures that the total flux of zonal momentum into the water column is $\tau_s(y)$. Distributing the wind stress over a "surface-forced layer," with specified thickness δ_s, relieves the model from resolving Ekman layers.

The bottom stress divergence is also represented as a body force $-r\gamma_b(z)(u\hat{\mathbf{x}} + v\hat{\mathbf{y}})$ in (1). This bottom drag force is applied over a layer of thickness $\delta_b \ll H$ using the bottom concentrated function:

$$\gamma_b(z) \equiv \frac{H}{\delta_b}\sqrt{\frac{2}{\pi}} e^{-(z+H)^2/2\delta_b^2}, \tag{5}$$

chosen to have unit vertical average. We use $\delta_b = 40$ m. The time scale r^{-1} controls the strength of the bottom drag and is the spindown time of the barotropic velocities. The eddy diffusivity and viscosity κ and ν represent small-scale mixing processes such as breaking internal gravity waves and mixed layer turbulence. Because the stresses are modeled as interior sources and sinks, the top and bottom boundary conditions are $\nu u_z = \nu v_z = 0$.

b. Buoyancy forcing

The thermal forcing at the surface $z = 0$ is applied with a fixed buoyancy boundary condition:

$$b(x, y, 0, t) = b_s(y), \tag{6}$$

and again we use the sinusoidal profile:

$$b_s(y) = -B\cos(2\pi y/L_y). \tag{7}$$

In the following we will always assume that B is positive.

Some earlier idealized studies (Karsten et al. 2002; Kuo et al. 2005) impose the buoyancy flux over part of the ocean surface. This fixed-flux limit is certainly appropriate when the buoyancy is determined by the salinity, but not for heat. For temperature, relaxation to an "apparent atmospheric temperature" approximates the air–sea heat exchange (Haney 1971), with a relaxation time that is generally more rapid than typical eddy-turnover times, and certainly much shorter than mean advection times. This rapid relaxation can be approximated with the prescription of the surface temperature value, and this is the limit that we consider. The bottom boundary condition is no flux:

$$\kappa b_z(x, y, -H, t) = 0.$$

c. Method of solution

The problem formulated in the previous section is solved with a finite-difference primitive equation model in a doubly periodic domain, described in Cessi and Fantini (2004). The horizontal resolution is 10 km, with a domain size of $L_x \times L_y = 2000$ km $\times$ 4000 km. The vertical resolution is variable, ranging from 7 m near the top and bottom, so as to resolve the vertical structures of γ_s and γ_b defined in (3) and (5), to 130 m in the center. The depth is $H = 2000$ m.

3. The mean circulation

The zonally reentrant geometry allows a simple and unambiguous decomposition of the dynamical variables in terms of mean and eddy components. The mean is defined as a zonal and time average, and it is denoted by an overbar:

$$\overline{u}(y, z) \equiv \int_0^{t_\infty}\int_0^{L_x} u(x, y, z, t)\frac{dx}{L_x}\frac{dt}{t_\infty}, \tag{8}$$

where t_∞ is long enough to remove the unsteadiness due to eddy fluctuations. The eddy part is denoted by a prime and is given by the difference

$$u' \equiv u - \overline{u}. \tag{9}$$

Once $\overline{b}(y, z)$ is known, the mean velocities are easily calculated using approximate analytic methods. This is because all our computations are in a regime where the contribution of the eddies to the momentum balance is small. In other words, the Reynolds stresses are negligible, because the typical eddy scale is substantially larger than the deformation radius. In summary, the mean velocity, $\overline{\mathbf{u}} = (\overline{u}, \overline{v}, \overline{w})$ is obtained by solving

$$\begin{aligned} -f\overline{v} &\approx \delta_s^{-1}\gamma_s(z)\tau_s(y) - r\gamma_b(z)\overline{u}, \\ f\overline{u} + \overline{p}_y &\approx 0, \\ \overline{p}_z &= \overline{b}, \quad \text{and} \\ \overline{v}_y + \overline{w}_z &= 0. \end{aligned} \tag{10}$$

The zonal flow $\overline{u}$ is obtained using thermal wind balance, $f\overline{u}_z = \overline{b}_y$, with the barotropic component constrained by the depth integral of the zonal momentum equation:

$$r\int_{-H}^{0} \gamma_b(z)\overline{u}(y, z)\, dz = \tau_s(y). \tag{11}$$

The mean meridional flow $\overline{v}$ vanishes in the interior (i.e., outside the top and bottom boundary layers).

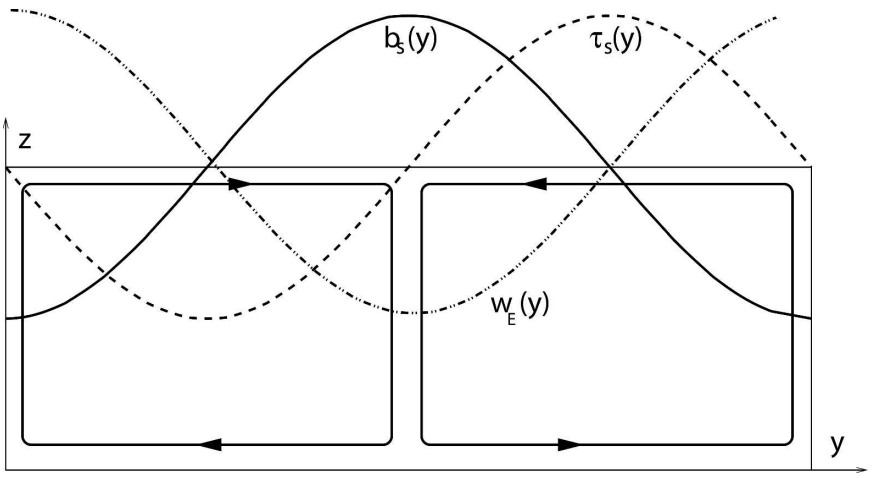

FIG. 1. A schematic diagram of the forcing and mean circulation for the thermally indirect cell configuration [$\tau > 0$, ϕ=0 in (2)]. The sinusoidal lines show the surface buoyancy (solid), wind stress (dashed), and Ekman pumping (dash–dotted). The direction of the mean meridional circulation in the y–z plane is given by the arrows. For the indirect case, the sign of the wind stress and of the Ekman pumping is opposite to that shown here, and the sense of the mean circulation is reversed.

Thus, the vertical velocity in the interior is independent of depth and is given by the Ekman velocity

$$w_E \equiv -f^{-1} d\tau_s/dy.$$

Direct versus indirect wind stress curl

As shown by (2), our meridionally periodic domain has always both westerlies and easterlies, and both positive and negative Ekman pumping. For $\tau > 0$ and $\phi = 0$, surface buoyancy decreases with y in the region of westerlies, while in the easterlies region buoyancy increases with latitude (cf. Fig. 1). In this configuration, the surface Ekman flow converges toward the region of high surface buoyancy while the return flow at depth is toward low buoyancy. The associated pattern of Ekman velocity pushes buoyant water down and sucks negatively buoyant water up, overturning the isopycnals. In the presence of weak diffusion the mean circulation creates a statically unstable stratification, and generates a thermally indirect cell. This configuration, qualitatively appropriate for the ACC, has been shown by several authors to generate eddies (Karsten et al. 2002; Cenedese et al. 2004; Gallego et al. 2004; Henning and Vallis 2005; Cessi et al. 2006). In particular, Cessi et al. (2006) show that the net buoyancy transport, when volume averaged, must be in the direction opposite to the surface buoyancy gradient. In other words for indirect wind stress curl, the mechanical forcing cannot force the net buoyancy transport to be in the direction of the mean meridional circulation (indicated by arrows in Fig. 1). Instead, eddies must counteract this upgradient buoyancy flow. At the same time, the pattern of Ekman pumping favors eddies energetically, because it raises the potential energy of the system, by bringing high (low) buoyancy fluid at a lower (higher) level in the water column.

In the next section we will explicitly show that "indirect" wind stress curls are associated with large amounts of potential energy that can be extracted by mesoscale eddies. Thus, for the indirect Ekman pumping shown in Fig. 1 both the buoyancy and the mechanical energy budgets require eddies.

If the winds are reversed [i.e., $\phi = \pi$ (with $\tau > 0$), still with $B > 0$ in (7)], the mean circulation is reversed, and it can establish a statically stable stratification in the presence of small diffusion. With this configuration the buoyancy budget does not require that eddies develop. We will show in the following that they do not, and that the absence of mesoscale time-dependent fluctuations is consistent with the mechanical energy balance for the eddies.

4. The mean buoyancy

Figures 2 and 3 show the mean buoyancies for indirect (Fig. 2) and direct (Fig. 3) wind stress curl for one set of parameter values. The surface distribution of buoyancy is deepened with no tilt in both cases. The typical vertical scale of $\overline{b}$, denoted by h, is much deeper with indirect wind stress curl than with the direct one. In the following we will show that the difference in the two cases is qualitative, not just quantitative, and the two configurations are in different regimes.

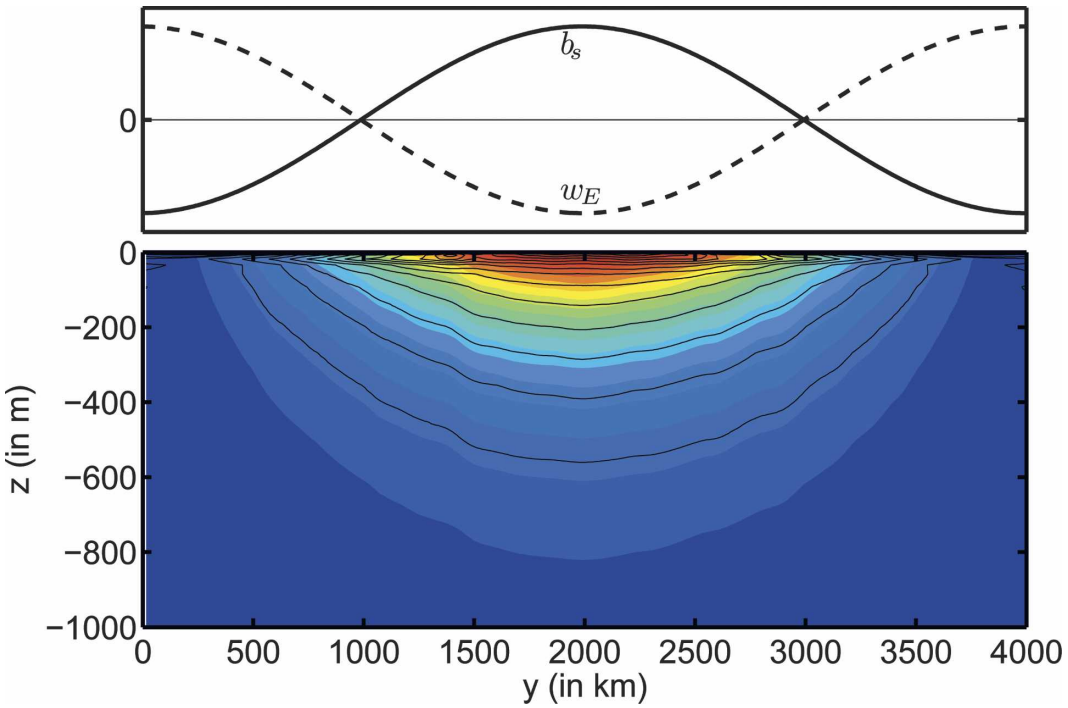

FIG. 2. (top) The surface forcings fields, $b_s(y)$ (solid line), and $w_E(y)$ (dashed line) for run 2 ($\phi = 0$). (bottom) The corresponding zonally and time-averaged buoyancy $\overline{b}(y, z)$ is shown in colors. The contour interval is 2×10^{-3} m^2 s^{-1}. The large-scale Ertel potential vorticity $\overline{b}_z(y, z)$ is shown in black. Below a surface trapped region, $\overline{b}$ and $\overline{b}_z$ are coincident.

The mean buoyancy is obtained by zonally averaging (1) and decomposing the flow into a mean and an eddy part. Outside of the top and bottom Ekman layers, $\overline{v} = 0$ and $\overline{w} = w_E$, so the interior buoyancy is governed by

$$(\overline{v'b'})_y + (\overline{w'b'})_z + w_E\overline{b}_z \approx \kappa\overline{b}_{zz}. \tag{12}$$

The interior balance is approximate because the horizontal diffusion terms have been neglected.

a. *The interior balance for indirect wind stress curl, $\tau > 0$, $\phi = 0$*

As discussed by many authors (Karsten et al. 2002; Marshall et al. 2002; Marshall and Radko 2003; Gallego et al. 2004; Kuo et al. 2005; Cessi et al. 2006) when $\tau > 0$ and $\phi = 0$, the main balance in the interior is between the terms on the left of (12), with the diabatic term on the right a negligible residual. Without eddies, the mean circulation tends to overturn the buoyancy surfaces, creating a statically unstable buoyancy distribution, which is then vertically homogenized by convection (or convective adjustment). A typical buoyancy profile in an eddyless model is shown in Henning and Vallis (2005, their Fig. 4), and it should be contrasted with the stably stratified profile obtained when eddies are allowed (shown in the same figure). The vertically homogenized laminar state is unstable to baroclinic disturbances that equilibrate to an amplitude such that the mean and eddy buoyancy transport are of the same order, and both much larger than the diapycnal mixing of buoyancy. This quasiadiabatic competition between the mean and eddy buoyancy transports generates a mean stratification that can be roughly described as

$$\overline{b} \approx (b_s + B)\exp(z/h) - B. \tag{13}$$

The model (13) satisfies the condition that the large-scale potential vorticity, $q = f\overline{b}_z$, is constant on mean isopycnals $\overline{b}$, which is what we see in the numerical computations (cf. the bottom panel in Fig. 2). This is a particular solution of the inviscid, nondiffusive thermocline equations, which require that potential vorticity and buoyancy are conserved following the flow (Pedlosky 1987, chapter 6.20). Although it is not possible to prove it rigorously, Rhines and Young (1982) have suggested that eddies tend to homogenize potential vorticity on buoyancy surfaces, and our computations confirm this prediction. When the zonally averaged Ertel potential vorticity (here approximated with $f\overline{b}_z$) is constant on buoyancy surfaces, it can be shown (cf. the appendix in Cessi et al. 2006) that the eddies have *zero* quasigeostrophic potential vorticity. For ed-

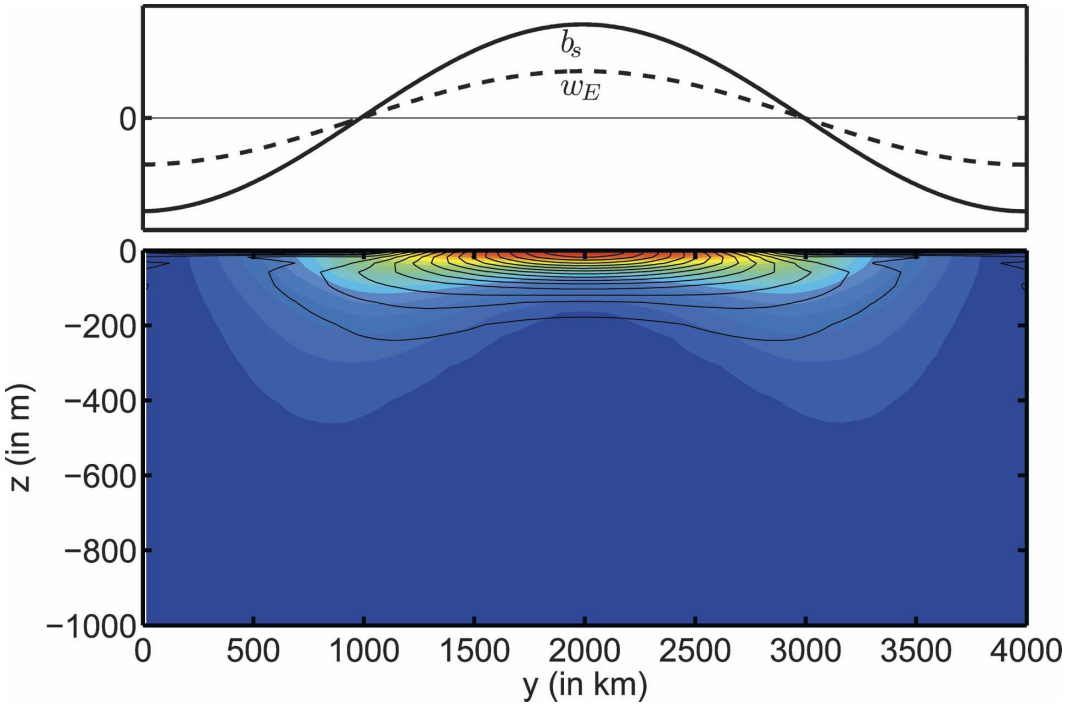

FIG. 3. Same as in Fig. 2, but for run 10 ($\phi = \pi$). In this configuration the potential vorticity contours cross the isopycnals in the whole thermocline region, an indication that the diabatic terms are important throughout the thermocline.

dies larger than the deformation radius, which satisfy the nondiffusive version of (12), this leads to eddy fluxes of buoyancy of the form $\overline{v'b'} = \tau_s(y)\overline{b}_z/f$. The essential point is that the vertical scale h characterizing $\overline{b}$ has an order of magnitude given by

$$h \sim B\tau/(f\overline{v'b'}). \tag{14}$$

To determine h in terms of the externally specified parameters, such as B, τ, and so on, a scaling for the eddy transport $\overline{v'b'}$ must be provided. In our configuration, with $\phi = 0$, Cessi et al. (2006) show that a good estimate can be obtained by using the relation

$$\overline{v'b'} \sim V\ell B/L_y, \tag{15}$$

where V is the typical barotropic eddy velocity, and ℓ is the eddy mixing length. As argued by several authors (Salmon 1980; Larichev and Held 1995; Cessi and Fantini 2004; Henning and Vallis 2005), it is the barotropic component of the eddies that is primarily responsible for the eddy buoyancy flux. The barotropic eddy velocity can be obtained from the eddy–energy balance in (31), which yields the following scaling for V:

$$V \sim \left(\frac{h\tau B}{HfL_y r}\right)^{1/2}. \tag{16}$$

No scaling for the mixing length ℓ consistent with the numerical results is offered by Cessi et al. (2006), so the thermocline depth is not completely determined in terms of the external parameters and is instead given by

$$h \sim L_y\left(\frac{rH\tau}{fB\ell^2}\right)^{1/3}. \tag{17}$$

Figure 4 shows h as a function of the diffusivity κ for the computations summarized in Table 1. The indirect case is denoted by the times sign.

As a practical measure of the thermocline depth h we use

$$h^2 \equiv [(\overline{b} - \tilde{b})^2]/[(\overline{b} - \tilde{b})_z^2], \tag{18}$$

where the basic stratification $\tilde{b}(z)$ is defined as

$$\tilde{b}(z) \equiv L_y^{-1}\int_0^{L_y} \overline{b}(y, z)\, dy. \tag{19}$$

The essential point is that h is independent of the diffusivity, although it depends on the spindown rate, r. In some of the computations shown in Fig. 4 r is varied *together* with κ (cf. Table 1) so a slope appears in h versus κ. However, the computations at fixed r and varying κ (runs 2 and 4) have approximately the same h. As detailed by Cessi et al. (2006) h is proportional to $r^{1/2}$ rather than the explicit dependence $r^{1/3}$ given in (17). This is because ℓ scales as $r^{-1/4}$, so that h ends up scaling as $r^{1/2}$.

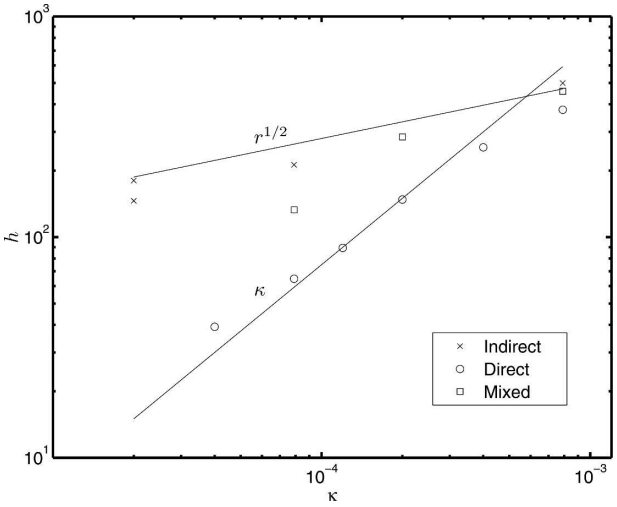

FIG. 4. The thermocline depth defined in (18) as a function of the diffusivity κ. The times signs are for indirect wind stress curl (runs 1–4), the circles are for direct wind stress curl (runs 5–11), and the squares are for the wind stress curl in quadrature with the surface buoyancy (runs 12–14). Notice from Table 1 that for runs 1–3 r varies with κ, such that $r/(\kappa)^{1/2}$ is kept fixed. Runs 2 and 4 have the same value of r but different κ, and h is almost the same. Runs 3 and 4 have the same value of κ but different r, and h differs substantially. Runs 9 and 10 (direct) have the same value of κ but different values of r and produce the same value of h.

TABLE 1. The parameter values for the primitive equation model in the doubly periodic configuration are $H = 2000$ m, $L_x = 2 \times 10^6$ m, $L_y = 4 \times 10^6$ m, $f = 10^{-4}$ s^{-1}, $B = 2 \times 10^{-2}$ m s^{-2}, $\tau = 1 \times 10^{-4}$ (m^2 s^{-2}), $P \equiv \nu/\kappa = 25$, and $\Delta x = \Delta y = 10.417$ km.

Run	κ (m^2 s^{-1})	ϕ	r (s^{-1})	h (m)	Symbol
1	8×10^{-4}	0	7.0×10^{-7}	499	×
2	8×10^{-5}	0	2.2×10^{-7}	213	×
3	2×10^{-5}	0	1.1×10^{-7}	146	×
4	2×10^{-5}	0	2.2×10^{-7}	180	×
5	8×10^{-4}	π	7.0×10^{-7}	378	○
6	4×10^{-4}	π	3.5×10^{-7}	255	○
7	2×10^{-4}	π	3.5×10^{-7}	148	○
8	1.2×10^{-4}	π	3.5×10^{-7}	89	○
9	8×10^{-5}	π	2.2×10^{-7}	65	○
10	8×10^{-5}	π	3.5×10^{-7}	65	○
11	4×10^{-5}	π	2.2×10^{-7}	39	○
12	8×10^{-4}	$-\pi/2$	7.0×10^{-7}	458	□
13	2×10^{-4}	$-\pi/2$	3.5×10^{-7}	284	□
14	8×10^{-5}	$-\pi/2$	2.2×10^{-7}	133	□

The scaling for h offered in (17) should be compared with other proposals in idealized channel geometries. All of these works, including the present, share the assumption of a quasi-adiabatic interior where the mean and eddy buoyancy fluxes balance. These assumptions lead to the scaling relation $\overline{v'b'} \sim \tau B/fh$. Moreover, all of the proposed scalings are unified by a common interpretation of the eddy fluxes of buoyancy in terms of an eddy closure of the form (15). In combining (15) with the scaling relation above, one obtains

$$h \sim \frac{\tau L_y}{fV\ell}. \tag{20}$$

The difference among these works resides in estimating the transfer velocity V and the mixing length ℓ in (20).

The interpretation of the laboratory and numerical experiments of Karsten et al. (2002), Marshall and Radko (2003), and Cenedese et al. (2004) revolves around arguments originally due to Green (1970). Green's assumption is that the eddy transfer velocity V scales with the *baroclinic* component of the zonally averaged zonal velocity $\overline{u}$, assumed to be in thermal-wind balance. Thus $V \sim Bh/(fL_y)$. The mixing length is taken as the external horizontal scale of the zonal flow, $\ell \sim L_y$. Putting these estimates into (20), Marshall and his collaborators obtain for the depth of the thermocline $h \sim (\tau L_y/B)^{1/2}$.

The calculations of Henning and Vallis (2005) retain the dependence of the Coriolis parameter on latitude, $f = f_0 + \beta y$, and include bottom relief, while our work is on the f plane and has a flat bottom. Henning and Vallis (2005)'s estimate of $V\ell$ in (20) stems from ideas rooted in the geostrophic turbulence literature. Thus, Henning and Vallis (2005) assume, as we do, that the eddy transfer velocity, V, is that of the *barotropic* eddies. Henning and Vallis (2005) make an equipartition assumption that the barotropic eddy kinetic energy is of the same magnitude as the eddy available potential energy: $V \sim (Bh)^{1/2}\ell/L_y$. The mixing length is associated with the largest eddy scale, identified with the Rhines scale, so that $\ell \sim (V/\beta)^{1/2}$. The resulting scaling for the depth of the thermocline is $h \sim (\tau L_y^2 f)^{2/5} B^{-3/5}$. The implicit assumption of Henning and Vallis (2005) is that β is the dominant mechanism to arrest the inverse cascade. Thus, in contrast to our view, the barotropic eddies are assumed to equilibrate at an amplitude that is independent of the explicit dissipation parameters, such as the bottom drag.

Our approach to estimating the eddy flux is also inspired by ideas from geostrophic turbulence theory, and we follow Henning and Vallis (2005) and Cessi and Fantini (2004) in identifying V as the barotropic eddy velocity. However, our numerical calculations do not support the assumption of equipartition of eddy energy between the baroclinic and barotropic modes. Instead we use the energy balance argument in section 5 to estimate the eddy transfer velocity V; this inevitably introduces the bottom drag r. Because our computations do not support the inertial hypothesis of Kolmogorov, we cannot use the arguments summarized in Smith et al. (2002) to estimate the drag-induced halting

scale, and ℓ remains unknown. The diagnosis of ℓ not shown here (cf. Cessi et al. 2006) indicates that the mixing length is considerably smaller than the domain scale L_y, it is larger than the deformation radius, and scales as $r^{-1/4}$. Thus, the numerical simulations are consistent with the scaling in (17).

b. *The interior balance for thermally direct wind stress curl, $\tau > 0$, $\phi = \pi$*

In this regime, it will be shown in the following section that eddies are not generated. It is then possible to assume that the eddy contribution can be omitted from (12), in which case we have the classical abyssal recipe balance between a mean upwelling velocity and diffusion (Munk 1966). The approximate solution that satisfies the boundary condition and is statically stable is

$$\overline{b} \approx -B + [b_s(y) + B]\exp(-w_E z/\kappa). \tag{21}$$

For this solution it is clear that the vertical scale of the mean buoyancy is

$$h \sim \kappa L_y f/\tau. \tag{22}$$

This diffusive boundary layer can only be maintained in the region of upwelling, where $w_E > 0$. In the region of downwelling, the laminar solution that satisfies the boundary conditions is simply

$$\overline{b} \approx b_s(y), \tag{23}$$

that is, a vertically homogenized solution, which is baroclinically unstable. In the direct case the laminar solution in (21) is valid in the region $-L_y/2 < y < L_y/2$, where the surface buoyancy is largest, while (23) applies where the buoyancy is small and convective motions are found. We find that the eddy activity is confined to this well-mixed convective region, and that it is weaker than in the indirect case. This relative weakness is possibly due to a replacement of eddy activity by upright convection. It is also possible that in this weakly stratified region the horizontal scale of the baroclinic eddies is below our resolution. As a result, the eddy energy is smaller for the direct wind stress than in the indirect case.

Figure 4 shows h defined in (18) for a series of numerical computations where both r and κ are varied (cf. Table 1). For direct wind stress (circles), h is approximately linear in κ and independent of the bottom drag as indicated by the solution in (21). The numerical solutions for indirect wind (times signs) agrees with the scaling (17), which requires the eddy flux as an essential element. In the following section we will show that the two configurations have qualitatively different energetics.

5. The energy balance

In this section the numerical results are interpreted in terms of the mechanical energy balance, by examining the sources of eddy energy as a function of the wind–buoyancy phase relation. An angular bracket denotes a volume and time average,

$$\langle A \rangle \equiv \int_0^{t_\infty} \int A(x, y, z, t) \frac{dV}{\mathcal{V}} \frac{dt}{t_\infty}, \tag{24}$$

where the total volume of the model ocean is $\mathcal{V} = L_x L_y H$.

Dotting $\mathbf{u}$ into the momentum equations and averaging over the volume gives the global kinetic energy budget

$$\delta_s^{-1}\langle \gamma_s \tau_s u \rangle + \langle wb \rangle = r\langle \gamma_b |\mathbf{u}|^2 \rangle + \langle \nu \|\nabla \mathbf{u}\|^2 \rangle. \tag{25}$$

Following Paparella and Young (2002) we obtain a more convenient expression for the total conversion between kinetic and potential energy, $\langle wb \rangle$. Multiplying the buoyancy equation by z and volume averaging we obtain

$$\langle wb \rangle = \langle \kappa \overline{b}_z \rangle. \tag{26}$$

Using (26) to eliminate $\langle wb \rangle$ in (25), the mechanical energy equation can be rewritten exactly as

$$\delta_s^{-1}\langle \gamma_s \tau_s \overline{u} \rangle + \langle \kappa \overline{b}_z \rangle = r\langle \gamma_b |\mathbf{u}|^2 \rangle + \langle \nu \|\nabla \mathbf{u}\|^2 \rangle. \tag{27}$$

The first term on the right of (27) is the dissipation of mechanical energy by bottom drag. This is the main sink of mechanical energy, and is always larger than the dissipation of mechanical energy by internal friction, $\langle \nu \|\nabla \mathbf{u}\|^2 \rangle = \langle \nu (u_x^2 + u_y^2 + u_z^2 + \upsilon_x^2 + \upsilon_y^2 + \upsilon_z^2) \rangle$. Thus, we neglect the final term in (27) from now on.

It is also useful to partition the mechanical energy balance into the contribution between mean and eddies. One readily finds the mean contribution:

$$-\sum_{i=1,2}\sum_{j=2,3} \langle u_i' u_j' \partial_{x_j} \overline{u}_i \rangle + \delta_s^{-1}\langle \gamma_s \tau_s \overline{u} \rangle + \langle \overline{w}\,\overline{b} \rangle = r\langle \gamma_b |\overline{\mathbf{u}}|^2 \rangle, \tag{28}$$

and eddy contribution

$$\sum_{i=1,2}\sum_{j=2,3} \langle u_i' u_j' \partial_{x_j} \overline{u}_i \rangle + \langle w'b' \rangle = r\langle \gamma_b |\mathbf{u}'|^2 \rangle. \tag{29}$$

In the Reynolds stress terms, we have used the notation $(x_1, x_2, x_3) = (x, y, z)$ and $(u_1, u_2, u_3) = (u, \upsilon, w)$. Notice that triple correlation terms vanish under the total volume average in $\langle\,\rangle$ and that in summing (28) and (29) we recover the total energy budget in (25).

The first terms on the left of (28) and (29) are the Reynolds stress conversions between the mean and the

eddies. To the extent that Reynolds stress work is negligible in the eddy equation we obtain $\langle w'b' \rangle \approx r\langle \gamma_b |\mathbf{u}'|^2 \rangle$. This approximation works well because the scale of the eddies is larger than the deformation radius, in which case the Reynolds contribution to the energy balance is negligible relative to the conversion of available potential energy. Using (26), and $\langle w'b' \rangle = \langle \kappa \overline{b}_z \rangle - \langle \overline{w}\,\overline{b} \rangle$ we obtain

$$\langle \kappa \overline{b}_z \rangle - \langle \overline{w}\,\overline{b} \rangle \approx r\langle \gamma_b |\mathbf{u}'|^2 \rangle. \tag{30}$$

Recalling that in most of the domain $w = w_E$, and specializing to the case of constant κ we find

$$\kappa H^{-1}\langle b_s + B \rangle - \langle w_E \overline{b} \rangle \approx r\langle \gamma_b |\mathbf{u}'|^2 \rangle. \tag{31}$$

The relation in (31) is the important result of this section: it illustrates the fundamentally different balances occurring in the indirect versus the direct regimes. For small diffusivity, it is tempting to neglect the first term on the left-hand side, and indeed this is a good approximation for the $\phi = 0$ configuration. This is the situation described by Gill et al. (1974): available potential energy is generated by Ekman pumping. This energy is transferred via baroclinic instability to mesoscale eddies. The right-hand side of (31) is the damping of the baroclinically driven eddies by bottom drag. The balance between production of eddy energy by "useful wind work" and dissipation is only possible for *negative* correlation between w_E and $\overline{b}$, that is, when Ekman pumping is at the latitudes of positive buoyancy and Ekman suction is in phase with negative buoyancy. This is the case for the indirect configuration. As detailed in Cessi et al. (2006) this approximate balance provides the scaling for the typical bottom velocity of the eddies, which, for $h \ll H$, is equivalent to the barotropic eddy speed in (16). Through the scaling provided by the eddy–energy balance we can estimate the typical eddy velocity V used in (15) and (16).

When the wind stress curl is reversed, the correlation between w_E and $\overline{b}$ is positive and the useful wind work in (31) becomes a *sink* of available potential energy rather than a source. This sink is balanced by the first term on the left side of (31), which is the work by buoyancy. However, this term is very small for realistic values of the diffusivity κ. Thus, the only way that a balance can be achieved is to have a thermocline depth that is linearly proportional to κ. This is the scaling in (22) given by the laminar solution in (21). In this regime, the dissipation of eddy kinetic energy by the bottom drag is a small residual, and the eddy field is very weak. With such a thin thermocline, the vertical shear of the zonal flow is in a diffusive boundary layer and eddies do not arise.

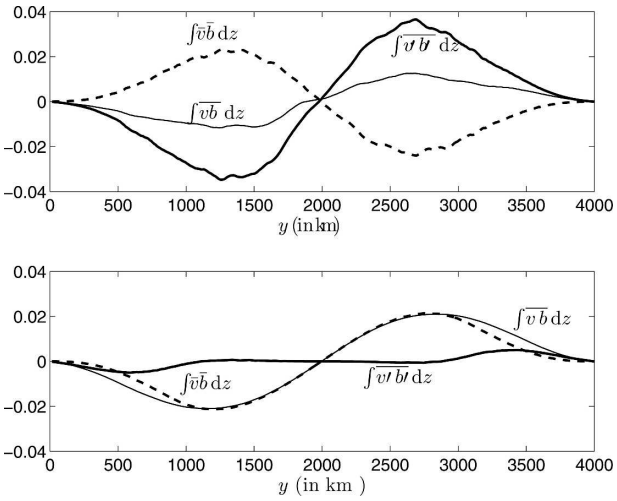

FIG. 5. The meridional buoyancy transport Q, defined in (32), as a function of latitude y for (top) run 2 (indirect wind stress curl) and (bottom) run 10 (direct wind stress curl). The net transport Q defined in (32) is plotted with a thin solid line. The contribution by the mean velocity is denoted by a thick dashed line, and the eddy component is denoted by a thick solid line.

6. Implications for heat transport

The two scalings for h described in the previous section are accompanied by two different regimes in the heat transport, proportional to the buoyancy transport Q, defined as

$$Q \equiv \int_{-H}^{0} \overline{v}\,\overline{b}\,dz. \tag{32}$$

It is useful to partition the contribution to Q into the mean $\overline{v}\,\overline{b}$ and eddy $\overline{v'b'}$ components. Figure 5 shows Q and its mean and eddy components for typical computations in the indirect (top panel) and direct (bottom panel) cases. For indirect wind stress curl, the net buoyancy transport is a small residual of the cancellation between the eddy and mean transport. For direct wind stress curl the net transport is larger and essentially determined by the mean component, while the eddy transport is small and confined to the low-buoyancy section of the domain.

The difference in the dynamics of the two cases leads to qualitatively different scalings of Q. In both cases, we can estimate the magnitude of Q by using the relation between the surface flux and the meridional transport obtained by integrating the buoyancy equation in x and z:

$$Q_y = \kappa \overline{b}_z(y, 0). \tag{33}$$

This relation states that the vertically and zonally integrated convergence of meridional buoyancy transport is balanced in steady state by the surface buoyancy flux. In our configuration, where the surface buoyancy is

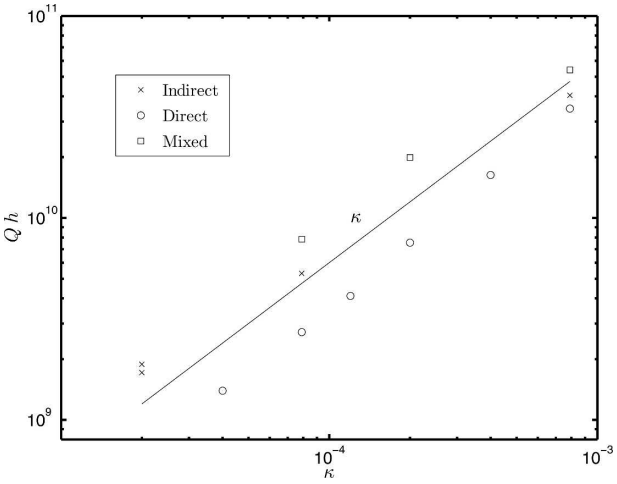

FIG. 6. The quantity Qh as a function of κ for all the runs in Table 1. The key is as in Fig. 4. The solid line has a slope of κ. The buoyancy transport Q is defined in (32).

specified, the surface flux is determined as part of the solution. The expression in (33) is useful because we can scale the right side from the interior buoyancy solution discussed in section 4 (i.e., $Q \sim \kappa BL_y/h$). The assertion that the interior vertical scale of the buoyancy can be used to estimate the surface flux will be detailed in the following section. The essential point is that, because h is independent of κ for the indirect case, the net heat transport is linearly proportional to the diffusivity, which controls the magnitude of the diabatic terms. Conversely, for the direct wind stress curl, h is linearly dependent on κ, so that the meridional buoyancy transport, proportional to the heat transport, becomes independent of the mixing coefficient.

In summary, it is argued that the heat transport should scale as

$$Q \sim \begin{cases} \kappa\left(\dfrac{fB^4\ell^2}{rH\tau}\right)^{1/3} & \text{indirect} \\ B\tau/f & \text{direct.} \end{cases} \tag{34}$$

To concisely support this scaling, Fig. 6 shows the product Qh for all the computations listed in Table 1. The times signs show the indirect case, and the circles show the direct case. The solid line has a slope of κ and is a reasonable fit to all the data.

7. The near-surface boundary layer

The interior balance considered in section 4 does not hold close to the surface, where a correction is necessary that takes into account, inter alia, the mean meridional Ekman flow. The necessity of a correction is evident both in the interior solution in the direct regime in (13) and in the laminar solution in (21), neither of which satisfy the condition that the integral over all latitudes of the surface flux vanishes:

$$\int_0^{L_y} \kappa \overline{b}_z(y,0)\, dy = 0.$$

In the following it is shown, at least for the laminar regime, that the surface correction is a weak one, where only the z derivative of $\overline{b}$ is corrected to leading order, but not $\overline{b}$ itself. Furthermore, the correction to the flux in this surface boundary layer does not alter the scaling estimate of $\overline{b}_z$ obtained from the interior solution. Cessi et al. (2006) advance similar arguments for the indirect regime, where eddies are essential.

In the surface layer the mean buoyancy in the laminar regime is governed by

$$\overline{\psi}_\eta \overline{b}_\zeta - \overline{\psi}_\zeta \overline{b}_\eta = \epsilon^{-1} \overline{b}_{\zeta\zeta}. \tag{35}$$

We have introduced the nondimensional spatial variables

$$\eta \equiv 2\pi y/L_y \quad \text{and} \quad \zeta \equiv z/\delta_s \tag{36}$$

and the Ekman layer meridional streamfunction

$$\overline{\psi} \equiv \sin\eta \int_\zeta^0 \gamma_s(s)\, ds. \tag{37}$$

The relation between $\overline{\psi}$ and the zonally averaged dimensional flow is given by

$$\overline{v} = -\frac{\tau}{f\delta_s}\overline{\psi}_\zeta \quad \text{and} \quad \overline{w} = \frac{2\pi\tau}{fL_y}\overline{\psi}_\eta. \tag{38}$$

The parameter ϵ, defined as

$$\epsilon \equiv \frac{2\pi\delta_s\tau}{\kappa L_y f}, \tag{39}$$

is the ratio of the Ekman layer depth to the depth of the thermocline, and it is considered small.

In the interior region, $\zeta \to -\infty$, $\overline{\psi}$ becomes independent of ζ, and the solution in (35) is

$$\overline{b} = -B + A(\eta)\exp(\epsilon\zeta\cos\eta), \tag{40}$$

with $A(\eta)$ determined by matching to the near-surface region. It will be shown shortly that the solution in (21) is recovered for the interior region.

Near the surface, we can solve (35) as a regular perturbation expansion in the small parameter ϵ:

$$\overline{b} = \overline{b}_0 + \epsilon\overline{b}_1 + \cdots. \tag{41}$$

The leading-order equation is $\overline{b}_{0zz} = 0$. The solution that satisfies the top boundary condition is simply $\overline{b}_0 = b_s(y)$. At next order $\overline{b}_1$ satisfies

$$-\overline{\psi}_\zeta \overline{b}_{0\eta} = \overline{b}_{1\zeta\zeta}. \tag{42}$$

The solution that satisfies the top boundary condition is

$$\overline{b}_1 = \Gamma(\eta)\zeta + \sin\eta b_{s\eta}\left[\zeta\int_{-\infty}^{\zeta}\gamma_s(s)\,ds + \int_{\zeta}^{0} s\gamma_s(s)\,ds\right], \tag{43}$$

where Γ is the interior flux. We now determine $A(\eta)$ and $\Gamma(\eta)$ by matching the outer limit ($\zeta \to -\infty$) of the surface solution with the inner limit ($\zeta \to 0$) of the interior solution in (40). To this end (40) is expanded up to $O(\zeta)$ and equated to the surface solution thus found:

$$-B + A(\eta)(1 + \epsilon\cos\eta\zeta) = b_s(\eta) + \epsilon[\Gamma(\eta)\zeta + \sin\eta b_{s\eta}\int_{-\infty}^{0} s\gamma_s(s)\,ds]. \tag{44}$$

We thus find

$$A = b_s + B + O(\epsilon) \quad \text{and} \tag{45}$$

$$\Gamma = (b_s + B)\cos\eta + O(\epsilon). \tag{46}$$

As advertised, the interior solution recovers (21) to $O(\epsilon)$. We are now in a position to calculate the leading-order surface flux as

$$\kappa\overline{b}_z(y,0) = \kappa\frac{\epsilon}{\delta_s}\overline{b}_{1\zeta}(\eta,0) = \frac{2\pi\tau}{L_y f}(\Gamma + \sin\eta b_{s\eta}) = -f^{-1}\frac{d}{dy}\{[b_s(y) + B]\tau_s(y)\}. \tag{47}$$

The surface flux is the divergence of the vertically integrated meridional transport of buoyancy:

$$\int_{-H}^{0}(\overline{v}\overline{b})_y\,dz.$$

The latter is given by the surface Ekman layer transport $-\tau_s/f$ times the surface buoyancy b_s plus the bottom Ekman layer transport τ_s/f (equal and opposite to the surface transport) times the bottom buoyancy $-B$. It is clear that the order of magnitude of the surface flux is the same as that of the interior one, Γ. The surface boundary layer corrects the interior flux so that it has zero latitudinal average, without altering its scaling.

8. A generic phase between the wind stress curl and the surface buoyancy

In this section we consider a situation that is intermediate between the ones considered so far (i.e., when the phase in the wind stress is $\phi = -\pi/2$). In this case, the sign of the wind work, $\langle w_E\overline{b}\rangle$ is not clear a priori: assuming that the surface buoyancy distribution is imparted at depth without substantial tilt, then the wind work is approximately zero. This is because for the first half of the domain we have upwelling and in the second half we have downwelling, which is equal and opposite, with a surface buoyancy distribution that is symmetric around the midlatitude: $\langle w_E b_s\rangle = 0$.

Figure 7 shows $\overline{b}$ and $f\overline{b}_z$ for a typical simulation in this regime. The thermocline is thinner in the half of the domain where there is Ekman suction, and the large-scale potential vorticity $f\overline{b}_z$ (in black lines) crosses the average isopycnals (in color). In this configuration the symmetry around the central latitude is broken, and the meridional distribution of buoyancy and potential vorticity reflects this broken symmetry.

In the southern region we have upwelling and reduced eddy activity, so the meridional buoyancy transport is dominated by the mean (Fig. 8). The suppression of eddies by upwelling occurs for two reasons: on one hand the mean circulation tends to flatten the isopycnals reducing the vertical shear where baroclinic instability can grow; on the other hand when the thermocline is reduced to a diffusive thickness, as in the scaling in (22), instability processes are halted by diffusion. Nevertheless, eddies are found in the southern portion of the domain (where $w_E > 0$), indicating that the relation between Ekman pumping (or useful wind work) and the eddies is not entirely local.

The phase between the wind stress curl and the buoyancy is such that the mean component of the transport is upgradient of the mean buoyancy distribution in parts of the southern region, a new feature that is not found in either of the symmetrical cases examined in section 4, and this upgradient transport is not effectively counteracted by the eddies.

In the northern half (downwelling) the northern buoyancy transport is dominated by eddies and it is everywhere downgradient of the vertically averaged $\overline{b}$. As a result, the meridional transport of buoyancy, *when volume averaged*, is downgradient of the surface buoyancy distribution, as required in equilibrium (Cessi et al. 2006). The eddy available potential energy $-\langle\overline{w}\overline{b}\rangle$ is positive: the tilt with depth of the thermocline implies that the positive contribution from the Ekman pumping outweighs the negative contribution from the Ekman suction.

Although h as defined in (18) is plotted in Fig. 4 for this generic phase, we do not attempt a scaling for this configuration, since we argue that different regimes exist in different parts of the basin. Indeed, Fig. 4 shows that the globally defined thermocline depth is intermediate between the well-defined regimes discussed in section 4.

9. Discussion

In the ocean available potential energy is produced by a combination of mechanical and buoyancy forcing

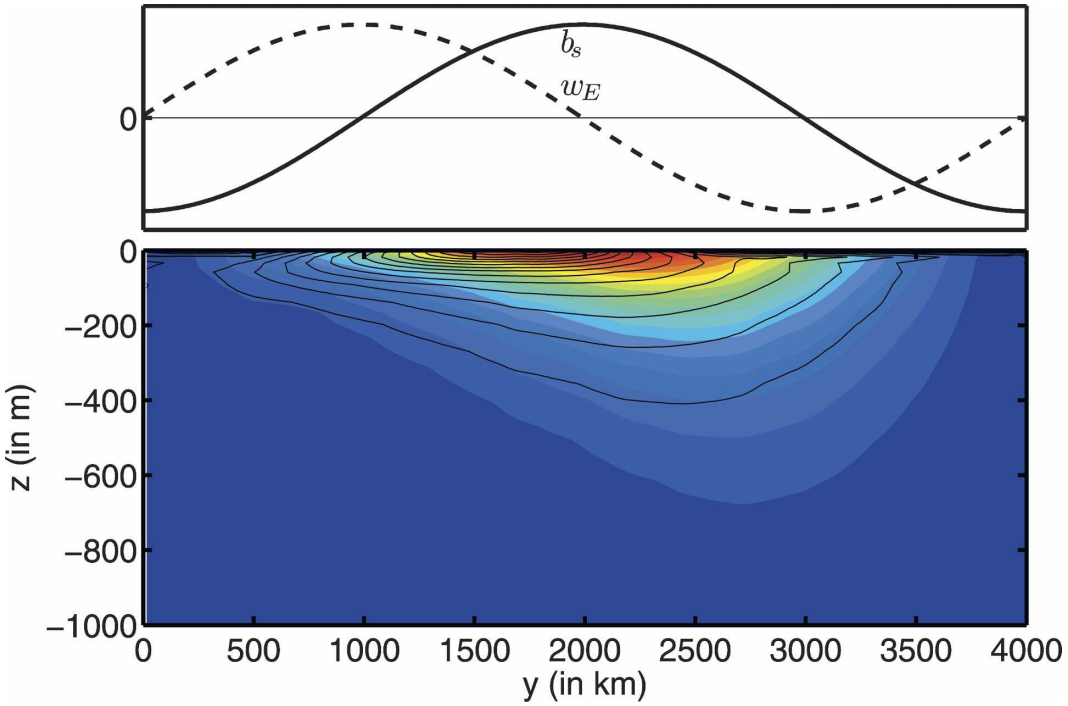

FIG. 7. Same as in Fig. 2, but for run 14 ($\phi = -\pi/2$). In the northern half of the domain (downwelling) $\overline{b}$ and $\overline{b}_z$ are coincident in the interior, while in the southern portion of the domain (upwelling) potential vorticity contours cross the isopycnals in the whole thermocline region.

(Gill et al. 1974). We find that the phase of the wind stress curl relative to that of the surface buoyancy distribution determines whether baroclinic eddies will develop, or whether the flow remains laminar. In particular, regions of upwelling combined with high surface buoyancy are unfavorable for eddy development because the mechanical forcing flattens isopycnals reducing the available potential energy. Furthermore, for $w_E > 0$ the thickness of the thermocline is reduced to a diffusive boundary layer, and diffusion suppresses the onset of baroclinic instability. Remarkably, Munk's (1966) abyssal recipe balance holds in regions of Ekman upwelling, even when eddies are allowed to exist.

This result is consistent with the observation that, generally speaking, eddy kinetic energy in the ocean is lower in the subpolar gyres (Stammer et al. 2006). However, it is at odds with the maxima in eddy kinetic energy found near the equator, which is also a region of upwelling. The equatorial region has of course other sources of variability, such as barotropic instability of the narrow equatorial currents system, and this could explain why so much eddy energy is found there. An alternative hypothesis is that baroclinic geostrophic turbulence on a β plane tends to concentrate eddy kinetic energy in low latitudes, where the Rossby deformation radius is largest (Theiss 2004). In the context of baroclinic eddies in the Tropics, the suppression of eddy development by upwelling documented in the present study would be opposed by the geostrophic turbulence tendency. If both these competing effects are operating in nature, then it appears that the free evolution of geostrophic turbulence is more fundamental than the control of available potential energy by Ekman pumping.

Not surprisingly, the thermocline is thinner in regions of upwelling than in regions of downwelling. Perhaps unintuitively, a thin, diffusive, eddyless thermocline is a very efficient environment for transporting heat pole-

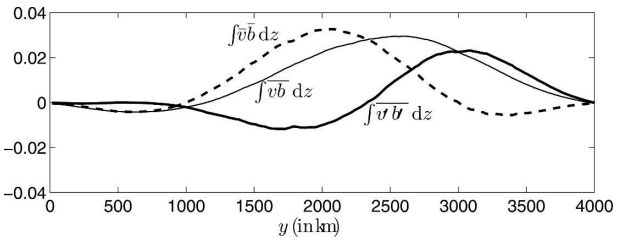

FIG. 8. The meridional buoyancy transport as a function of latitude y for run 14. The net transport Q, defined in (32), is plotted with a thin solid line. The contribution by the mean velocity is denoted by a thick dashed line, and the eddy component is denoted by a thick solid line.

ward: this is because a thin thermocline has a large surface flux, given the proximity of all buoyancy classes to the air–sea interface. Furthermore, the work by upwelling-favorable wind is productively used by the mean circulation to carry heat poleward, while the energy induced by downwelling-favorable wind is largely expended against bottom drag by eddy motion necessary to counteract the equatorward heat transport by the mean, and to restratify the water column.

It is thus tempting to ascribe the maximum in poleward oceanic heat transport observed at approximately 15°N and 15°S (Trenberth and Caron 2001) to the mechanical control summarized above, even though our results are obtained in a longitudinally reentrant geometry and on the f plane. A parallel study is under way to verify that the same mechanism is also operating in a β-plane, semienclosed basin, which is a geometry more appropriate to the low and midlatitude oceans.

Our results indicate the necessity of including information about the eddy energy balance in parameterizations of eddy buoyancy fluxes. The energy balance is one of the constraints where the control on eddy development by the combined mechanical and buoyancy forcing is explicitly stated. The success of our scaling predictions for the depth of the thermocline obtained using the eddy energy balance in (31) encourages us to use this relation to constrain parameterizations of eddy fluxes. Work to implement these ideas in the parameterization of eddy fluxes of buoyancy is in progress and will be reported later.

Acknowledgments. This research was supported by the Office of Science (BER) U.S. Department of Energy, Grant DE-FG02-01ER63252. We acknowledge the National Center for Computational Sciences (NCCS) at Oak Ridge National Laboratory for computational resources used in support of this project. John Marshall and an anonymous referee are gratefully acknowledged for their constructive suggestions.

REFERENCES

Cenedese, C., J. Marshall, and J. A. Whitehead, 2004: A laboratory model of the thermocline depth and exchange fluxes across circumpolar fronts. *J. Phys. Oceanogr.,* **34,** 656–667.

Cessi, P., and M. Fantini, 2004: The eddy-driven thermocline. *J. Phys. Oceanogr.,* **34,** 2642–2658.

——, W. R. Young, and J. A. Polton, 2006: Control of large-scale heat transport by small-scale mixing. *J. Phys. Oceanogr.,* **36,** 1877–1894.

Gallego, B., P. Cessi, and J. C. McWilliams, 2004: The Antarctic Circumpolar Current in equilibrium. *J. Phys. Oceanogr.,* **34,** 1571–1587.

Gent, P., J. Willerbrand, T. McDougall, and J. McWilliams, 1995: Parameterizing eddy-induced tracer transports in ocean circulation models. *J. Phys. Oceanogr.,* **25,** 463–474.

Gill, A. E., J. S. A. Green, and A. J. Simmons, 1974: Energy partition in the large-scale ocean circulation and the production of mid-ocean eddies. *Deep-Sea Res.,* **21,** 499–528.

Green, J., 1970: Transfer properties of the large-scale eddies in the general circulation of the atmosphere. *Quart. J. Roy. Meteor. Soc.,* **96,** 157–185.

Haney, R. L., 1971: Surface thermal boundary condition for ocean circulation models. *J. Phys. Oceanogr.,* **1,** 241–248.

Henning, C. C., and G. K. Vallis, 2005: The effects of mesoscale eddies on the stratification and transport of an ocean with a circumpolar channel. *J. Phys. Oceanogr.,* **35,** 880–896.

Karsten, R., H. Jones, and J. Marshall, 2002: The role of eddy transfer in setting the stratification and transport of a circumpolar current. *J. Phys. Oceanogr.,* **32,** 39–54.

Kuo, A., A. Plumb, and J. Marshall, 2005: Transformed Eulerian-mean theory. Part II: Potential vorticity homogenization, and the equilibrium of a wind-and buoyancy-driven zonal flow. *J. Phys. Oceanogr.,* **35,** 175–187.

Larichev, V. D., and I. M. Held, 1995: Eddy amplitudes and fluxes in a homogeneous model of fully developed baroclinic instability. *J. Phys. Oceanogr.,* **25,** 2285–2297.

Marshall, J., and T. Radko, 2003: Residual-mean solutions for the Antarctic Circumpolar Current and its associated overturning circulation. *J. Phys. Oceanogr.,* **33,** 2341–2354.

——, H. Jones, R. H. Karsten, and R. Wardle, 2002: Can eddies set ocean stratification? *J. Phys. Oceanogr.,* **32,** 26–38.

Maximenko, N. A., B. Bang, and H. Sasaki, 2005: Observational evidence of alternating zonal jets in the World Ocean. *Geophys. Res. Lett.,* **32,** L12607, doi:10.1029/2005GL022728.

Munk, W., 1966: Abyssal recipes. *Deep-Sea Res. I,* **24,** 1259–1262.

Paparella, F., and W. R. Young, 2002: Horizontal convection is non-turbulent. *J. Fluid Mech.,* **466,** 205–214.

Pedlosky, J., 1987: *Geophysical Fluid Dynamics.* 2d ed. Springer Verlag, 710 pp.

Rhines, P. B., and W. R. Young, 1982: Homogenization of potential vorticity in planetary gyres. *J. Fluid Mech.,* **122,** 347–367.

Richards, K. J., N. A. Maximenko, F. O. Bryan, and H. Sasaki, 2006: Zonal jets in the Pacific Ocean. *Geophys. Res. Lett.,* **33,** L03605, doi:10.1029/2005GL024645.

Salmon, R., 1980: Baroclinic instability and geostrophic turbulence. *Geophys. Astrophys. Fluid Dyn.,* **15,** 165–211.

Smith, K. S., G. Boccaletti, C. C. Hennings, I. Marinov, C. Y. Tam, I. M. Held, and G. K. Vallis, 2002: Turbulent diffusion in the geostrophic inverse cascade. *J. Fluid Mech.,* **469,** 13–48.

Stammer, D., C. Wunsch, and K. Ueyoshi, 2006: Temporal changes in ocean eddy transports. *J. Phys. Oceanogr.,* **36,** 543–550.

Theiss, J., 2004: Equatorward energy cascade, critical latitude, and the predominance of cyclonic vortices in geostrophic turbulence. *J. Phys. Oceanogr.,* **34,** 1663–1678.

Treguier, A., I. Held, and V. Larichev, 1997: Parameterization of quasigeostrophic eddies in primitive equation ocean models. *J. Phys. Oceanogr.,* **27,** 567–580.

Trenberth, K., and J. Caron, 2001: Estimates of meridional atmosphere and ocean heat transports. *J. Climate,* **14,** 3433–3443.